

Initiation of ballooning instability by reconnection in the near-Earth plasma sheet

P. Zhu¹, J. Raeder², K. Germaschewski², and C. C. Hegna¹

¹Department of Engineering Physics, University of Wisconsin-Madison, Madison, WI 53706, USA

²Department of Physics, University of New Hampshire, Durham, NH 03824, USA

Abstract. In this work, an alternative scenario for the substorm onset process is proposed, based on ideal ballooning stability analysis of the near-Earth plasma sheet during the March 23, 2007 THEMIS substorm event. In this scenario, the ballooning instability is initiated by the magnetic reconnection in the near-Earth plasma sheet, which in turn directly contributes to the trigger of a full onset. Using the solar wind data from WIND satellite observation for the substorm event as an input at dayside, we reconstructed a sequence of global magnetospheric configurations around the substorm onset by means of OpenGGCM simulation. These simulations have reproduced most of the salient features, including the onset timing, observed in the THEMIS substorm event (Raeder et al., 2008). The local ballooning instability criterion is evaluated for the near-Earth plasma sheet region when the configuration attains a quasi-static equilibrium condition. Our analysis of the evolution of the near-Earth magnetotail region during this substorm event reveals a correlation between the breaching of the ballooning stability condition and the substorm onset in both temporal and spatial domains. The analysis suggests that the Earthward bulk plasma flow induced by the reconnection event in the near-Earth plasma sheet, leads to the pressure build-up and creates a favorable condition for the initiation of the ballooning instability in that same region.

and simulations. On the other hand, it appears that the trigger mechanism may actually involve multiple entangled processes (Voronkov et al., 2004). In this work, we suggest an alternative scenario that involves multiple processes for the substorm onset, based on a ballooning analysis of the near-Earth plasma sheet during the March 23, 2007 THEMIS substorm event.

Most previous investigations of ballooning instabilities in the near-Earth magnetotail have been carried out under the assumption of a magnetostatic magnetosphere that is absent of either flow or reconnection (Miura et al., 1989; Hameiri et al., 1991; Lee and Wolf, 1992; Pu et al., 1992; Ohtani and Tamao, 1993; Hurricane et al., 1995, 1996, 1997; Bhattacherjee et al., 1998; Cheng and Lui, 1998; Lee, 1999; Wong et al., 2001; Crabtree et al., 2003; Zhu et al., 2003; Cheng and Zaharia, 2004; Schindler and Birn, 2004; Zhu et al., 2004, 2007). In reality, the magnetosphere exhibits persistent convection and reconnection activities in the magnetotail region, which is often intermittent, as evidenced by the presence of bursty bulk flows (BBF) in both observations and simulations. The major processes in the near-Earth plasma sheet, ballooning, reconnection, and plasma bulk flow, each may have contributed indispensably to the onset of a substorm. The roles of each, and the interactions among them, may hold a key to understanding the trigger mechanism of substorm onset.

Recent observations from the multi-satellite mission THEMIS of the March 23, 2007 substorm event (hereafter referred to as the THEMIS substorm event) provide a unique opportunity for us to examine more closely the roles of ballooning instability and magnetic reconnection in the triggering of a substorm onset in a dynamically evolving magnetospheric configuration (Angelopoulos, 2008; Keiling et al., 2008). Using WIND solar wind data for the THEMIS substorm event, a sequence of global magnetospheric configurations have been reconstructed around the substorm onset by means of OpenGGCM simulations (Raeder, 2003).

1 Introduction

Conventional scenarios of the substorm onset event invoke either current disruptions at the near-Earth magnetotail or magnetic reconnection processes in the middle magnetotail. Both scenarios have been built on suggestive but sometimes ambiguous observational and theoretical evidence (See, for example, (Lui, 2003)). The ambiguity results in part from the lack of sufficient resolution in data, in both observations

Correspondence to: P. Zhu (pzhu@wisc.edu)

These simulations have reproduced most salient features of the observation (Raeder et al., 2008). Our local ballooning analysis of the near-Earth magnetotail configurations reconstructed from OpenGGCM simulations starts to reveal the role of magnetospheric convection and bulk plasma flow, the interaction between reconnection and ballooning instability, and the correlation between the breaching of the ballooning stability criterion and the substorm onset. From those analyses, an alternative scenario has emerged in which the reconnection process in the near-Earth plasma sheet, through the resulting Earthward plasma flow, is able to initiate a ballooning instability, which in turn directly contributes to a full disruption of that region.

2 Simulation Setup

The OpenGGCM simulation used in this study covers a spatial domain of $x : [20, -500], y : [-36, 36], z : [-36, 36]$ where the GSM coordinates are used and normalized by the Earth radius (R_E). The size of the nonuniform Cartesian grid is $630 \times 200 \times 300$. In the near-Earth plasma sheet region ($x : [-5, -40], y : [-5, 5], z : [-5, 5]$, unit: Earth radius), which is of primary interest for this paper, the typical grid spacings are in the ranges of $0.145 < (\Delta x) < 0.147$, $\Delta y \sim 0.25$, and $\Delta z \sim 0.16$. The grid spacings minimize around $y = 0$ and $z = 0$ planes, and increase monotonically in the tailward direction. The major simulation results remain qualitatively similar at higher spatial resolution. To reconstruct the THEMIS March 23, 2007 substorm event, the WIND solar wind data at the upstream of bow shock is imposed as the dayside boundary conditions. The ionosphere boundary conditions are determined by the Coupled Thermosphere Ionosphere Model (CTIM) (Fuller-Rowell et al., 1996).

3 Simulation Results

The maximum electron precipitation energy flux for discrete aurora from simulation indicates that the start of the first aurora intensification occurs shortly before 10:45 UT, consistent with the time series of Knight potential and ground magnetic perturbation (Fig. 1). Whereas the timing of the first intensification in simulation is slightly earlier than that recorded by THEMIS ground and in-situ observations (which is around 10:54 UT), comparisons of many other features of the event have shown considerable agreement (Raeder et al., 2008). The WIND data upstream of the bow shock suggests the northward turning of the magnetic field at the day side magnetopause occurs later at $\sim 11:10$ UT (Fig. 1)(Raeder et al., 2008).

We now take a closer look at four representative snapshots of the near-Earth magnetotail configurations from 10:10 UT to 10:43 UT prior to the first aurora intensification. In particular we focus on the series of pressure and tailward flow

patterns within the domain $x : [-5, -40], z : [-5, 5]$ in the meridional plane (Fig. 2).

Around 10:10 UT, the ionosphere and ground magnetic activity levels are low, and the near-Earth region ($-x \sim 10 - 20 R_E$) of the plasma sheet is moderately stretched, as seen from the pressure pattern. The plasma sheet stretching and thinning reaches the maximum extent at about 10:15 UT, with the thinnest point located around $12 R_E$. Soon afterward, the pressure contours at 10:35 UT and 10:43 UT indicate the formation and recession of a plasmoid-like structure in the tailward direction. Before the formation of the plasmoid (10:10 UT and 10:15 UT), the pressure profile in the near-Earth region is flat along x direction, but the peak value of the pressure starts to increase from 700 pP to 900 pP. After the plasmoid formation (10:35 UT and 10:43 UT), there is a dramatic steepening of the pressure profile in the region $-x \lesssim 10 R_E$, with the peak pressure value reaching 2300 pP.

During the same period, a weak bipolar flow, in both Earthward and tailward directions, starts to appear at 10:10 UT and becomes prominent at 10:15 UT, with the stagnation site located around $x = -10 R_E$ in the equatorial plane, as seen in the tailward flow contours. The stagnation site, along with the flow pattern, steadily recedes tailward, reaching $x = -17 R_E$ at 10:43 UT. The formation of the bipolar flow coincides with the thinning of the plasma sheet, and the initial stagnation site locates at the thinnest section of the plasma sheet near $x = -10 R_E$. The development of the bipolar flow pattern and the plasmoid-like structure indicate that the occurrence of a reconnection event in the near-Earth plasma sheet around $x = -10 R_E$ well before the first substorm intensification.

The initial near-Earth reconnection event at 10:15 UT results in a partial dipolarization and a tailward flow in the region $-x \lesssim 10 R_E$. One major consequence of the tailward flow induced by the reconnection is a dramatic pressure build-up in that same region at 10:35 and 10:43 UT. As shown next, that in turn initiates the ballooning instability of the near-Earth plasma sheet.

4 Ballooning Analysis

We use the conventional local dispersion relation

$$\Gamma^2 = -\Gamma_{\text{ben}}^2 + \Gamma_{\text{int}}^2, \quad (1)$$

to evaluate the ballooning instability of the near-Earth plasma sheet at the above four representative times. Here, Γ is the linear growth rate, $\Gamma_{\text{ben}}^2 \equiv k_{\parallel}^2 u_A^2 \lesssim (u_A/R_E)^2$ represents the line bending strength, $\Gamma_{\text{int}}^2 \equiv 2\rho^{-1} B \kappa_{\Psi} (dp/d\Psi)$ measures the pressure gradient drive due to unfavorable magnetic curvature (which we refer to as ‘‘interchange drive’’ in the rest of this paper), Ψ denotes the magnetic flux function defining the configuration, κ_{Ψ} the normal component of magnetic curvature, ρ the mass density, p the pressure, u_A the Alfvén

speed, B the magnitude of magnetic field, and k_{\parallel} the parallel wavenumber.

The local ballooning stability criterion in (1) is valid for configurations that are quasi-static. An appropriate form of the quasi-static condition is given by

$$\frac{|\mathbf{J} \times \mathbf{B} - \nabla p|}{\rho L_{\text{eq}} \Gamma^2} \ll 1, \quad (2)$$

the left hand side of which measures the ratio of the instability growth time to the configuration evolution time. This condition is well satisfied in the substorm growth phase in the near-tail region as reconstructed from simulation. Here \mathbf{J} is the plasma current, and $L_{\text{eq}} \sim R_{\text{E}}$ is the configuration scale length. In addition, for a conservative estimation of the line-bending stabilization, a maximum value of $k_{\parallel} \sim R_{\text{E}}^{-1}$ is assumed, which indicates a strong localization of the ballooning structure along the field line. Hence, the influence of ionosphere boundary and the plasma compression are ignored in (1).

The interchange drive Γ_{int}^2 and the line bending strength Γ_{ben}^2 are evaluated along the $y = 0, z = 0$ line in the equatorial and meridional planes, for each of the four time slices prior to the first substorm intensification (Fig. 3). At all times, the near-Earth magnetotail is ballooning stable in the region that is Earthward of the inner plasma sheet edge ($-x \lesssim 7.5 R_{\text{E}}$) due to strong dipole field and tailward-increasing pressure profile.

At 10:10 UT, only the region $13 R_{\text{E}} \lesssim -x \lesssim 17 R_{\text{E}}$ is weakly ballooning unstable because of a slightly enhanced interchange drive due to an increased magnetic curvature of the moderately stretched plasma sheet in the equatorial plane. At 10:15 UT, the entire near-tail and mid-tail region becomes marginally stable to ballooning instability, although the balance between interchange and line bending is different in the near-tail than in the mid-tail. The previous interchange drive peak at $x \sim -15 R_{\text{E}}$ disappeared due to pressure profile flattening, while the peak moved to $x \sim -10 R_{\text{E}}$ due to a slightly steepening of pressure profile there. However, the line bending strength is enhanced even more in the $x \sim -10 R_{\text{E}}$ region as the result of a moderate dipolarization. As mentioned earlier, both the pressure steepening and the dipolarization are induced by the initial reconnection event.

The interchange drive peaked around $x \sim -10 R_{\text{E}}$ continues to grow because of the continuing pressure steepening induced by the Earthward flow. At 10:35 UT, the growth of the interchange drive starts to surpass that of the line bending strength in that same near-tail region. By 10:43 UT, the near-tail region between $-7.5 R_{\text{E}}$ and $-14 R_{\text{E}}$ becomes strongly ballooning unstable, where the interchange drive is significantly enhanced while the line bending strength has remained at a relatively low level. After 11:00 UT, analysis indicates the interchange drive (line bending strength) starts to decrease (increase), and the near-tail region becomes marginally ballooning stable again.

The above development of ballooning properties shows a close correlation between the breaching of local ballooning instability criterion and the initial onset of the substorm event in both time and location. The Earthward bulk flow in the near-Earth tail appears to play a profound role by connecting and coupling the near-Earth tail reconnection and ballooning processes. Our simulation and analysis indicate that it is the Earthward flow generated by the near-tail reconnection event that leads to the build-up of the pressure gradient and the surge of the ballooning instability. The ensuing full onset process could be the direct outcome of the sudden rise of ballooning instability in the $-x = 7 - 15 R_{\text{E}}$ region.

5 Conclusions

In summary, a local ballooning analysis has been applied to the near-Earth magnetotail configurations obtained from OpenGGCM simulations for the THEMIS substorm event on March 23, 2007. Simulation and analysis indicate that the full onset event is closely correlated to the breaching of ballooning criterion in both time and space. The Earthward bulk flow induced by a reconnection event in the near-Earth plasma sheet region appears to help set up a favorable condition for the onset of a robust ballooning instability by building up the pressure gradient in that region. The ballooning instability could serve as an immediate trigger of the near-Earth current sheet disruption and the full onset process. Our analysis leads to an alternative scenario that may resemble both the near-Earth neutral-line model (McPherron et al., 1973) and the near-Earth current-sheet-disruption model (Lui et al., 1988) for substorm onset. In fact, the new alternative scenario has also the potential to integrate the two previous models into a unified near-Earth trigger, in-out expansion paradigm of substorm onset. It is worth noting that the initial near-Earth reconnection event in simulation occurs near a B_z minimum where the B_z is sufficiently weak but nonzero, and the reconnection process does not have to form an X-line in that region since a tearing instability can arise in presence of a weak but finite B_z (Sundaram and Fairfield, 1997; Sundaram, 2008). Only after the reconnection site recedes to the mid-tail region does an X-line start to appear. That is what has been observed in the highly stretched thin plasma sheet region near the B_z minimum in our simulation, which may hold the key to unifying the two previous onset models. The significance of the formation of a B_z minimum in the near-Earth plasma sheet was previously noted by Erickson (1992).

The local ballooning analysis in this letter is a first step aimed at identifying the roles of convection, ballooning, and reconnection in a substorm onset process, to lowest and dominant order. The favorable results in this work encourage further global ballooning analysis that involves solving the eigenmode equations along each flux tube under exact

boundary conditions, which will be reported in subsequent publications.

Acknowledgements. This research is supported by NSF Grant No. ATM-0542954. Computations were performed in NERSC (DOE Contract No. DE-AC03-76SF00098), on the Zaphod Beowulf cluster (NSF grant ATM-0420905), and through NSF TeraGrid resources provided by SDSC. P. Zhu is grateful for discussions with Prof. A. Bhattacharjee.

References

- Angelopoulos, V.: The THEMIS mission, *Space Sci. Rev.*, doi:10.1007/s11214-008-9336-1, 2008.
- Bhattacharjee, A., Ma, Z. W., and Wang, X.: Ballooning instability of a thin current sheet in the high-Lundquist-number magnetotail, *Geophys. Rev. Lett.*, 25, 861–864, 1998.
- Cheng, C. Z. and Lui, A. T. Y.: Kinetic ballooning instability for substorm onset and current disruption observed by AMPTE/CCE, *Geophys. Rev. Lett.*, 25, 4091–4094, 1998.
- Cheng, C. Z. and Zaharia, S.: MHD ballooning instability in the plasma sheet, *Geophys. Rev. Lett.*, 31, L06 809, doi:10.1029/2003GL018823, 2004.
- Crabtree, C., Horton, W., Wong, H. V., and Van Dam, J. W.: Bounce-averaged stability of compressional modes in geotail flux tubes, *J. Geophys. Res.*, 108, 1084, doi:10.1029/2002JA009555, 2003.
- Erickson, G. M.: A Quasi-Static Magnetospheric Convection Model in Two Dimensions, *J. Geophys. Res.*, 97, 6505–6522, 1992.
- Fuller-Rowell, T. J., Rees, D., Quegan, S., Moffett, R. J., Co-drescu, M. V., and Millward, G. H.: A coupled thermosphere-ionosphere model (CTIM), in: STEP Report, edited by Schunk, R. W., p. 217, Scientific Committee on Solar Terrestrial Physics (SCOSTEP), NOAA/NGDC, Boulder, Colorado, 1996.
- Hameiri, E., Laurence, P., and Mond, M.: The ballooning instability in space plasmas, *J. Geophys. Res.*, 96, 1513–1526, 1991.
- Hurricane, O. A., Pellat, R., and Coroniti, F. V.: The stability of a stochastic plasma with respect to low frequency perturbations, *Phys. Plasmas*, 2, 289–293, 1995.
- Hurricane, O. A., Pellat, R., and Coroniti, F. V.: Instability of the Lembége-Pellat equilibrium under ideal magnetohydrodynamics, *Phys. Plasmas*, 3, 2472–2474, 1996.
- Hurricane, O. A., Fong, B. H., and Cowley, S. C.: Nonlinear magnetohydrodynamic detonation: Part I, *Phys. Plasmas*, 4, 3565, 1997.
- Keiling, A., Angelopoulos, V., Larson, D., Lin, R., McFadden, J., Carlson, C., Bonnell, J. W., Mozer, F., Glassmeier, K.-H., Auster, U., Mende, S., Frey, H., Roux, A., LeContel, O., Frey, S., Phan, T., Donovan, E., Russell, C. T., Mann, I., Liu, W., Li, X., Fillingim, M., Parks, G., Yumoto, K., Shiokawa, K., and Raeder, J.: Correlation of substorm injections, auroral modulations, and ground Pi2, *Geophys. Rev. Lett.*, 35, L17S22, doi:10.1029/2008GL033969, 2008.
- Lee, D.-Y.: Stability analysis of the plasma sheet using Hall magnetohydrodynamics, *J. Geophys. Res.*, 104, 19993–19999, 1999.
- Lee, D.-Y. and Wolf, R. A.: Is the Earth's magnetotail balloon unstable?, *J. Geophys. Res.*, 97, 19 251–19 257, 1992.
- Lui, A. T. Y.: Cause of magnetospheric substorms, *Plasma Phys. Control. Fusion*, 45, 841–852, 2003.
- Lui, A. T. Y., Lopez, R. E., Krimigis, S. M., McEntire, R. W., Zanetti, L. J., and Potemra, T. A.: A Case Study of Magnetotail Current Sheet Disruption and Diversion, *Geophys. Rev. Lett.*, 15, 721–724, 1988.
- McPherron, R. L., Russell, C. T., and Aubry, M. P.: Satellite Studies of Magnetospheric Substorms on August 15, 1968, 9. Phenomenological Model for Substorms, *J. Geophys. Res.*, 78, 3131, 1973.
- Miura, A., Ohtani, S., and Tamao, T.: Ballooning instability and structure of diamagnetic hydromagnetic waves in a model magnetosphere, *J. Geophys. Res.*, 94, 15 231–15 242, 1989.
- Ohtani, S. and Tamao, T.: Does the ballooning instability trigger substorms in the near-Earth magnetotail?, *J. Geophys. Res.*, 98, 19 369, 1993.
- Pu, Z. Y., Korth, A., and Kremser, G.: Plasma and magnetic field parameters at substorm onsets derived from GEOS 2 observations, *J. Geophys. Res.*, 97, 19 341, 1992.
- Raeder, J.: Global Geospace Modeling: Tutorial and Review, in: Space Plasma Simulation, edited by J. Büchner, Dum, C. T., and Scholer, M., Springer Verlag, Berlin Heidelberg New York, 2003.
- Raeder, J., Larson, D., Li, W., Kepko, L., and Fuller-Rowell, T.: OpenGCM Simulations for the THEMIS Mission, *Space Sci. Rev.*, doi:10.1007/s11214-008-9421-5, 2008.
- Schindler, K. and Birn, J.: MHD stability of magnetotail equilibria including a background pressure, *J. Geophys. Res.*, 109, A10 208, doi:10.1029/2004JA010537, 2004.
- Sundaram, A. K.: Tearing instabilities driven by nonideal effects in the tail plasma sheet, *Phys. Plasmas*, 15, 052 901, doi:10.1063/1.2911691, 2008.
- Sundaram, A. K. and Fairfield, D. H.: Stability of resistive MHD tearing and ballooning modes in the tail current sheet, *J. Geophys. Res.*, 102, 19 913–19 926, doi:10.1029/97JA01241, 1997.
- Voronkov, I. O., Donovan, E. F., Dobias, P., Prosofin, V. I., Jankowska, M., and Samson, J. C.: Late growth phase and breakup in the near-Earth plasma sheet, in: Proceedings of the 7th International Conference on Substorms (ICS-7), Levi, Finland, 2004, p. 140, 2004.
- Wong, H. V., Horton, W., Van Dam, J. W., and Crabtree, C.: Low frequency stability of geotail plasma, *Phys. Plasmas*, 8, 2415–2424, 2001.
- Zhu, P., Bhattacharjee, A., and Ma, Z. W.: Hall magnetohydrodynamic ballooning instability in the magnetotail, *Phys. Plasmas*, 10, 249–258, 2003.
- Zhu, P., Bhattacharjee, A., and Ma, Z. W.: Finite- k_y ballooning instability in the near-Earth magnetotail, *J. Geophys. Res.*, 109, A11 211, doi:10.1029/2004JA010505, 2004.
- Zhu, P., Sovinec, C. R., Hegna, C. C., Bhattacharjee, A., and Germaschewski, K.: Nonlinear ballooning instability in the near-Earth magnetotail: Growth, structure, and possible role in substorms, *J. Geophys. Res.*, 112, A06 222, doi:10.1029/2006JA011991, 2007.

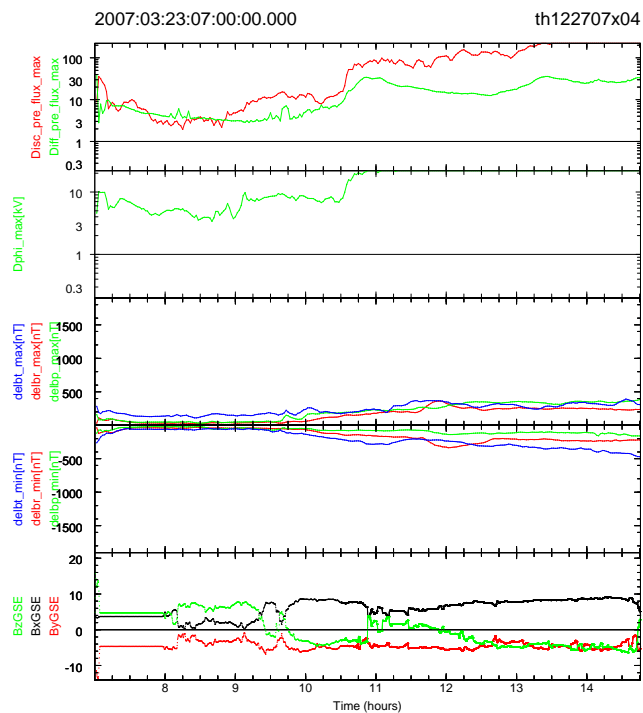


Fig. 1. Time series of ionosphere parameters during 08:00 UT ~14:00 UT from simulation: Discrete and diffuse auroral electron precipitation energy flux [mW/m^2] (first panel); maximum Knight potential (second panel); maximum (third panel) and minimum (fourth panel) ground magnetic perturbations; magnetic field at upper stream location (16,0,0) of bow shock (fifth panel).

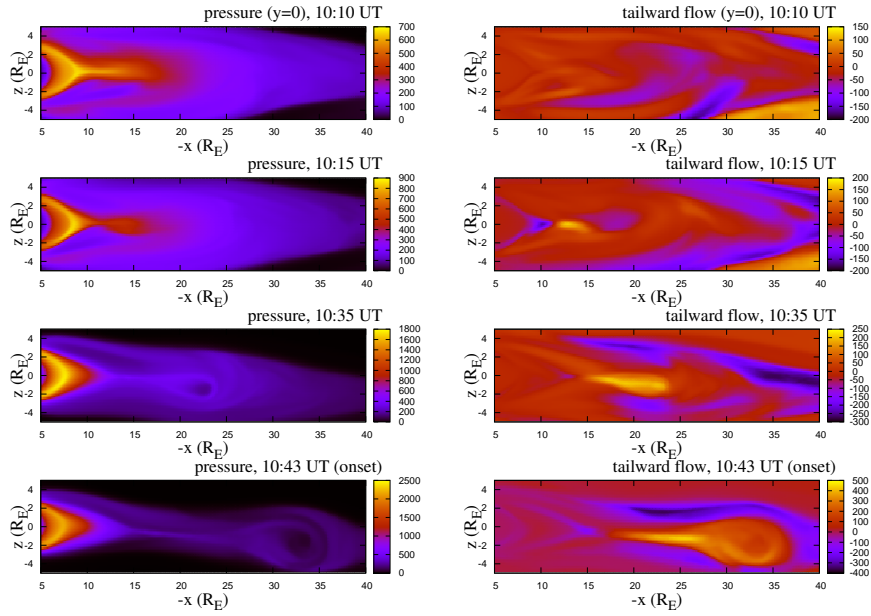


Fig. 2. Pressure (left column) and tailward flow (right column) patterns in meridional plane at four time slices prior to the first substorm intensification.

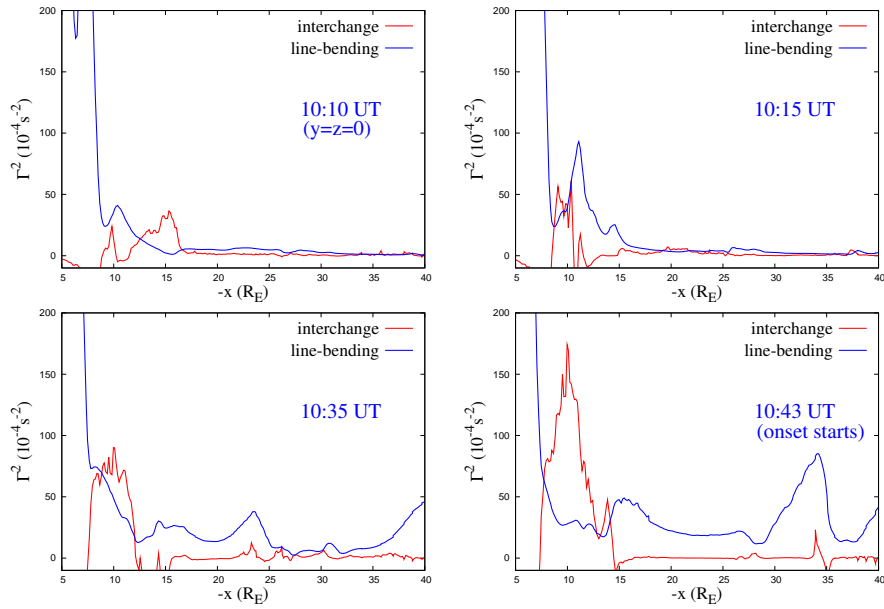


Fig. 3. Interchange drive Γ_{int}^2 and line bending strength Γ_{ben}^2 along line $y = z = 0$ in the near-Earth tail region at four representative times prior to the first substorm intensification.